GPS Solutions (2024) 28:118
https://doi.org/10.1007/s10291-024-01657-z

ORIGINAL ARTICLE

Quality monitoring of real-time PPP service using isolation forest-based residual anomaly detection

Xingxing Li[1] · Da Liang[1] · Xin Li[1,2] · Jiande Huang[1] · Jiaqi Wu[1] · Hailong Gou[1]

Received: 19 December 2023 / Accepted: 9 April 2024 / Published online: 1 May 2024

Abstract

In order to meet the time-critical and high-precision positioning demands of massive market applications, real-time Precise Point Positioning (PPP) technology has been continuously developed and can achieve a high level of accuracy now. Beyond precision, it is also crucial to ensure the security and stability of real-time high-precision positioning services. Nevertheless, there are few studies that addressed the fault detection and exclusion (FDE) of real-time PPP correction service to protect users from potential faults in the GNSS satellites. This paper introduces a new real-time products quality monitoring method that could effectively identify the potential fault of GNSS satellite corrections using an unsupervised learning algorithm and provide means to alert the real-time PPP users. The ambiguity-fixed Un-differenced Carrier-phase Residual Statistics (UCRS) of large-scale regional stations are first constructed to reflect the status of satellite corrections accurately. A machine learning technique, known as Isolation Forest, is employed to identify outliers in the UCRS to detect situations of potential satellite faults. Then, the UCRS alarm factors are transmitted to users for PPP processing with a modified weighting scheme based on alert information. Experimental validation utilizing 30 monitoring stations in China demonstrates a detection success rate exceeding 95% for orbit faults larger than 5 cm and clock faults larger than 0.2 ns. It is also proved that this method can effectively identify orbit and clock jump in real-time GNSS products that cause additional positioning errors. With the alert information broadcasted by the server, the PPP after FDE (PPP-FDE) presents a significant accuracy improvement of 27–71% compared with traditional PPP processing.

Keywords Quality monitoring · Real-time PPP · Ambiguity resolution · UCRS · Fault detection and exclusion

Introduction

The surge in demand for high-precision positioning provided by Global Navigation Satellite Systems (GNSS) has captured widespread attention, especially in applications such as autonomous car navigation and precision agriculture (European GNSS Agency 2019). Precise Point Positioning (PPP), recognized as a prominent technology within the GNSS, is capable of achieving global high-precision positioning using a single receiver (Malys and Jensen 1990; Zumberge et al. 1997; Kouba and Héroux 2001). The announcement by the International GNSS Service (IGS) (Dow et al. 2009) regarding the availability of real-time precise satellite orbit and clock in 2012 significantly sparked interest in real-time PPP techniques. Over the past decade, continuous enhancements have been witnessed in real-time PPP technology, including multi-frequency and multi-GNSS fusion (Li et al. 2018, 2021; Geng et al. 2020) and ambiguity resolution (Geng and Bock 2013; Li et al. 2014, 2019, 2023). As of now, real-time PPP can provide global positioning services with centimeter-level accuracy (İlçi and Peker 2022).

In certain real-world navigation applications, achieving high-accuracy positioning is not the sole requirement; the results generated by positioning must also be reliable and trustworthy (Zhang et al. 2023). Real-time PPP heavily relies on precise satellite orbit and clock corrections. At present, the real-time satellite products are available with high accuracy. However, it is inevitable that there are outliers or accuracy degradations in the real-time precise satellite products. Once these corrections contain substantial errors or inaccuracies due to system malfunctions

✉ Xin Li
xinli@sgg.whu.edu.cn

[1] School of Geodesy and Geomatics, Wuhan University, Wuhan 430079, China

[2] Hubei Luojia Laboratory, Wuhan 430079, China

or outliers, they could significantly impair the accuracy of positioning (El-Mowafy 2018). Currently, none of the real-time products from International GNSS Service (IGS) real-time service or its real-time Analysis Center (RTAC) is provided along with quality information (Ji et al. 2022). Therefore, the quality monitoring of real-time satellite products has become crucial, and it is urgent to establish a robust real-time product quality monitoring system. Such a system should possess the capability to detect and identify potential faults, promptly broadcast alert information to users, and ensure the continuity and stability of positioning.

The commercial company Trimble has developed an integrity monitoring module that detects real-time correction products (pre-broadcast and post-broadcast) in two steps, based on carrier phase residual modeling, monitors the entire data transmission chain, and generates alarms promptly (Weinbach et al. 2018). Wang and Shen (2020) proposed an integrity monitoring method for wide-area precision positioning system, and the fault simulation experiments for clock error correction proved that the method can monitor step and drift faults in the correction. Ji et al. (2022) proposed a method based on quality control theory to monitor real-time satellite orbit and clock products using a network of monitoring stations and evaluated GFZ real-time products, which proved to be accurate and effective in detecting problematic satellites. However, for potential sub-decimeter faults in real-time products, there is an urgent need for a more accurate and adaptive quality monitoring scheme, and its contribution to real-time PPP processing needs to be carefully studied. Meanwhile, as real-time PPP becomes more and more widely used, it is necessary to provide quality information on real-time satellite orbits and clock products.

This contribution proposes a new server-side quality monitoring scheme to accurately identify satellite orbit and clock anomalies and further enhance positioning performance for real-time PPP. This method employs the Isolation Forest machine learning algorithm (Liu et al. 2008) to identify outliers in Un-differenced Carrier-phase Residual Statistics (UCRS), facilitating the detection and identification of satellite orbit and clock potential faults. With real-time data from 30 stations distributed in China, this study analyzes fault detection and exclusion (FDE) of GNSS orbit and clock products and further evaluates its impact on positioning results.

After the introduction, we first introduce the carrier phase residual analysis based on the PPP AR model. On this basis, we describe in detail a real-time products quality monitoring method for detecting UCRS anomalies using Isolation Forest. Then, we will introduce the specific design of experiments and present a detailed analysis of anomaly detection results as well as the PPP after FDE results. Finally, we present our conclusions and discuss potential avenues for further research.

Method

This section introduces the retrieval of carrier phase residuals from the PPP-AR model. Subsequently, the satellite UCRS is constructed, and its outlier detection method using the Isolation Forest is presented. Finally, the design and workflow of the real-time products quality monitoring system are detailed.

Carrier phase retrieval from undifferenced PPP AR

For a multi-GNSS system, the linearized observation model of Un-Difference and Un-Combined (UCUD) PPP can be expressed as follows.

$$l^s_{r,j} = \boldsymbol{u}^s_r \cdot \boldsymbol{r}_r - \mathrm{d}T^s + \mathrm{d}t_r - \kappa_{js} \cdot I^s_{r,1} + m^s_r \cdot Z_r + \lambda_{\mathrm{js}} N^s_{r,j} + \lambda_{\mathrm{js}}(b_{\mathrm{rs},j} - b^s_j) + \varepsilon^s_{r,j} \tag{1}$$

$$p^s_{r,j} = \boldsymbol{u}^s_r \cdot \boldsymbol{r}_r - \mathrm{d}T^s + \mathrm{d}t_r + \kappa_{\mathrm{js}} \cdot I^s_{r,1} + m^s_r \cdot Z_r + (d_{\mathrm{rs},j} - d^s_j) + e^s_{r,j} \tag{2}$$

where $p^s_{r,j}$ and $l^s_{r,j}$ are the observations for pseudorange and carrier phase, respectively; the superscript s represents the satellite, the subscripts r and j represent the receiver and the frequency; $\boldsymbol{u}^s_r$ is the unit vector from the receiver to the satellite; $\boldsymbol{r}_r$ denotes the coordinates of receiver; $\mathrm{d}t_r$ refers to the receiver clock at the time of signal reception; $\mathrm{d}T^s$ is the satellite clock at the time of signal transmission; $\kappa_{js} \cdot I^s_{r,1}$ is the ionospheric delay between the satellite and receiver, where κ_{js} is a conversion parameter, $\kappa_{\mathrm{js}} = \lambda_j^2/\lambda_1^2$; Z_r represents the zenith tropospheric delay and m^s_r is the projection function along the signal propagation path; $d_{r,j}$ is the code delay between signal generation at the satellite end to its departure from the transmitting antenna; d^s_j is the code delay between signal reception at the antenna of receiver to its processing by the signal correlator; λ_j is the carrier wavelength of frequency j; $N^s_{r,j}$ is the carrier phase ambiguity for frequency j; $b_{r,j}$ and b^s_j refer to the carrier phase delay at the receiver and satellite side, respectively; $e^s_{r,j}$ and $\varepsilon^s_{r,j}$ refer to the measurement noise of pseudorange and phase observations, respectively. There are additional error sources, such as relativistic effects, phase wind up, antenna phase center variations, and tidal loading, which can be corrected using established models and thus are not included in the equation above.

With the precise orbit, clock and phase bias corrections, PPP AR can be achieved with the estimable parameters including the three-dimensional coordinates of the

receiver, receiver clock, slant ionospheric delay, zenith tropospheric wet delay, and integer ambiguity. Given the combination of multi-GNSS systems, intersystem bias (ISB) also should be considered.

$$X = \begin{pmatrix} \boldsymbol{r}_r & \mathrm{d}t_r & I_r^s & Z_r & N_r^s & ISB \end{pmatrix}^T \tag{3}$$

$$y = \mathrm{B}\mathrm{X} + \varepsilon \tag{4}$$

where (4) is obtained by combining (1) and (2) according to the estimated parameters in (3); y represents the observations, B refers to the design matrix of the estimated parameters, and ε is the measurement noise. After the PPP AR, the optimal value $\hat{X}$ of the estimated parameters can be calculated. The residuals v can be expressed as follows.

$$v = B\hat{x} - (y - y^0) \tag{5}$$

where $\hat{x}$ denotes the difference between $\hat{X}$ and X^0; X^0 represents the initial value of the estimated parameter; y^0 represents the approximate value of y calculated by substituting X^0 into (4).

For real-time PPP, precise orbit and clock products are generally applied for error correction. However, faults may arise in these real-time precise products due to system malfunctions or prediction outliers. Typically, these faults manifest within the residuals, allowing for the analysis of residual distribution regularity as a means to detect potential issues. Given the critical significance of the carrier phase in achieving high-precision positioning, this study focuses predominantly on the examination of carrier phase residuals.

A meticulous analysis of carrier phase residuals is critical for the facilitation of quality monitoring. Ideally, carrier phase residuals should conform to a Gaussian zero-mean distribution. The statistical analysis of carrier phase residuals is conducted utilizing data from 34 stations, employing static PPP AR solutions acquired from CNES real-time precise products. The Quantile–Quantile Plots method was employed for judging the distribution of carrier phase residuals by comparing the quantiles of two probability distributions. Figure 1 depicts the distribution of carrier phase residuals for select satellites from the BDS, Galileo, and GPS systems. Here, the red line signifies a zero-mean Gaussian distribution, while the green line represents the residual distribution for each satellite's carrier phase. Close alignment between the green line and the red line suggests adherence of carrier phase residuals to a Gaussian zero-mean distribution. Observation reveals that the central segments of carrier phase residuals across satellites from all systems closely approximate a Gaussian zero-mean distribution. However, the quantiles of carrier phase residuals surpass the quantiles of the Gaussian distribution in the tail distribution. This discrepancy indicates that constraining the tail distribution of carrier phase residuals using a Gaussian distribution permits the identification of potential satellite faults.

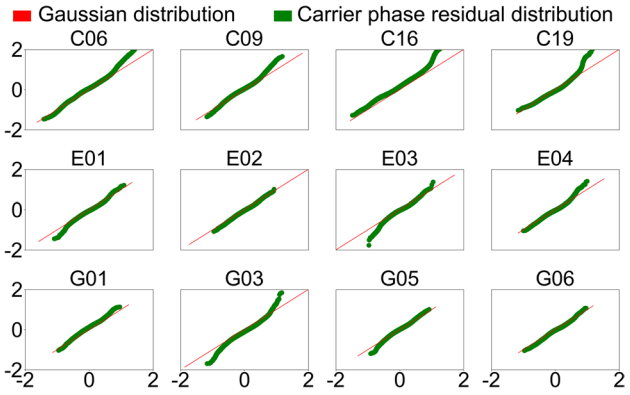

Fig. 1 Carrier phase residual distribution of satellite in GPS\GAL\BDS, with zero-mean Gaussian distribution

Detecting anomalies in satellite UCRS using isolation forest algorithm

In the quality monitoring module, the carrier phase residuals obtained by PPP AR are used to calculate the UCRS of the satellite. The Un-differenced Carrier-phase Residual Statistics (UCRS) are defined as monitoring parameter. It is employed to monitor variations in the distribution of satellite carrier phase residuals, referring to the expression form of the User Range Accuracy (URA) (Wang et al. 2013, 2015), defined as follows:

$$\mathrm{UCRS}^s = (|\mu^s| + K \cdot \sigma^s)/K \tag{6}$$

where μ^s and σ^s represent the mean and standard deviation of the carrier phase residuals for satellite s, respectively. K is the Gaussian quantile corresponding to the integrity risk P, $K = f^{-1}(1 - P)$, and $f^{-1}(\cdot)$ is the inverse of the normally distributed accumulation function (Wang et al. 2015). Here $P = 2 \times 10^{-2}/h$, $K = 2.33$. If the satellite UCRS is significantly higher than the normal value, it indicates that either the mean or the standard deviation of the residuals for the satellite's carrier phase does not conform to the expected distribution. Consequently, it is considered that the satellite may have experienced a fault at this moment.

After obtaining UCRS for a specific satellite at the current epoch, it is necessary to create a dataset by combining the UCRS for this satellite with the UCRS from some previous normal epochs. The dataset is subjected to anomaly detection using the Isolation Forest. If the UCRS for the

satellite in the current epoch is identified as an anomaly, the satellite is considered a problematic satellite.

After obtaining UCRS for a specific satellite at the current epoch, it is necessary to create a dataset by combining the UCRS for this satellite with the UCRS from some previous normal epochs. The dataset is then anomaly detected using a data anomaly detection method. If the UCRS of a satellite in the current epoch is identified as an anomaly, the satellite is considered problematic. Compared with the traditional data anomaly detection method based on mathematical statistics, the Isolation Forest algorithm is more suitable for real-time data anomaly detection because the Isolation Forest algorithm does not require actual data when building the initial model, and does not require distance or density calculation, with less memory occupation, fast speed, and guaranteed accuracy. Therefore, we chose the Isolation Forest algorithm as the tool for UCRS anomaly detection.

The Isolation Forest is an unsupervised anomaly detection method commonly used to identify anomalous data within a dataset. In the Isolation Forest, anomalous data points are defined as easily isolated outliers, meaning they are sparsely distributed and far from the densely clustered points. Typically, the number of anomalous data points is much smaller than the number of normal data points, and these anomalies exhibit certain distinct characteristics that differentiate them from normal data (Liu et al. 2008). Figure 2 shows the process of anomaly detection in Isolation Forest. Isolation forests do not rely on distance or density-based measurements to identify anomalies, so they are fast and computationally inexpensive.

The Isolation Forest comprises several Isolation Trees. Each Isolation Tree divides the overall dataset into smaller datasets by recursively splitting the data. The process of partitioning the small dataset at each step forms the nodes of the tree. Assuming that T is a node in an Isolation Tree, which can be in one of two states: it's either a leaf node with no child nodes or an internal node with two child nodes (T_l, T_r).

An Isolation Tree is constructed according to the difference of features to segment the dataset. This process is repeated recursively until one of the following conditions is met: the tree reaches a maximum height limit, a node has only one sample, or all samples in a node have the same feature values. The number of times that a sample point is split, which is the number of edges a sample point passes from the root node to a leaf node, is called the path length $h(x)$ of the sample point x.

The task of anomaly detection is to provide a ranking that reflects the degree of anomaly, and the commonly used sorting method is to sort based on the anomaly score of the sample points. The anomaly score is related to the path length of a sample point. The longer the path length, the more difficult it is to distinguish a sample point, indicating that it is more likely to be normal. Conversely, a shorter path length suggests that a sample point is easier to distinguish and is more likely to be anomalous. Given a dataset with n sample points, the average path length of the tree can be computed as:

$$c(n) = 2H(n-1) - (2(n-1)/n) \tag{7}$$

where $H(i)$ represents the harmonic number, which can be estimated as $\ln(i) + 0.5772156649$. $c(n)$ is the average path length for a given number n of samples, and it is utilized to standardize the path length of the samples. The anomaly score s for sample x is defined as:

$$s(x, n) = 2^{-\frac{E(h(x))}{c(n)}} \tag{8}$$

where $E(h(x))$ is the average of $h(x)$ from a collection of Isolation Trees. This anomaly score reflects the degree of

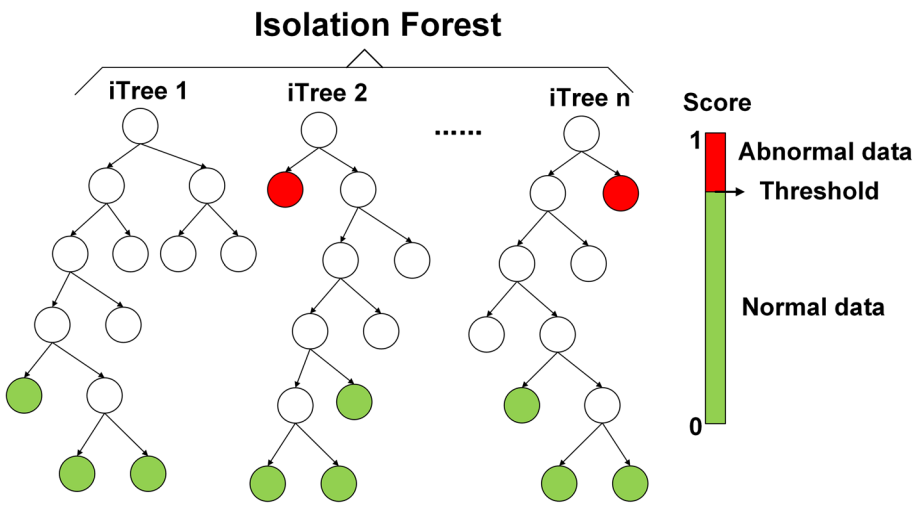

Fig. 2 Isolation Forest anomaly detection process

anomaly for sample point x, with higher values indicating a higher likelihood of being an anomaly.

In summary, the closer the score is to 1 and the shorter the path length, the easier it is for the sample to be separated, which means there is a greater difference from normal data and a higher probability of abnormal data; when the score is closer to 0 and the path length is longer, it indicates that the sample is less likely to be separated and has a higher probability of being normal data. Finally, by establishing a threshold for abnormal scores, it is possible to differentiate abnormal data from normal data.

According to this method, we can judge whether the UCRS of each satellite in the current epoch is abnormal, so as to determine whether the satellite is a problematic satellite. All problematic satellites and their UCRS are packaged together to form alert information, which is then broadcast.

UCRS-based weighting scheme

Users can perform PPP after FDE (PPP-FDE) by receiving alert information. In PPP-FDE, it is necessary to update the weights for problematic satellites. Taking satellite s as an example, the weight factor a^s for the satellite is computed as follows:

$$a^s = \left(\frac{\mathrm{UCRS}_0^s}{\mathrm{UCRS}^s} \right)^2 \tag{9}$$

where UCRS_0^s represents the statistical average of UCRS for satellite s in the most recent week, and UCRS^s denotes the UCRS for satellite s at the current epoch. Subsequently, the weights of the problematic satellite s are updated.

$$(\sigma^s)^2 = a^s (\sigma_0^s)^2 \tag{10}$$

where $(\sigma_0^s)^2$ represents the a priori precision of satellite observations, encompassing pseudorange and carrier phase observations.

Within the PPP process, for the satellites identified as problematic, this method is employed to reduce the weight assigned to these satellites. This method helps to mitigate the impact of problematic satellites on the positioning solution, thereby enhancing the overall quality of the positioning.

Quality monitoring system framework

In order to detect and identify potential faults in precise products, we propose a framework for a quality monitoring system. The overall design is depicted in Fig. 3. The quality monitoring system consists of the server and user parts. The server detects and identifies potential faults on satellites by receiving data from monitoring stations to obtain alert information and broadcast it. At the user, a weight scheme based on UCRS is used to downgrade the problematic satellites in the alert information, so that the PPP results after trouble removal can be obtained.

At the server, the observations from the monitoring stations are passed to the Data Processing Center for data preprocessing. At the same time, the real-time precise products and the real-time UPD products are received for PPP AR, to obtain the carrier phase residuals. Then, these residuals are passed into the UCRS calculation module to calculate the UCRS of all satellites in the current epoch according to (6). For each satellite, the UCRS of the current epoch is combined with the previous UCRS series to form a dataset, which will be used for anomaly detection in Isolation Forest. If the detection result is abnormal, it is determined that the satellite is problematic at this epoch; otherwise, UCRS is added to the previous UCRS series. Subsequently, all the

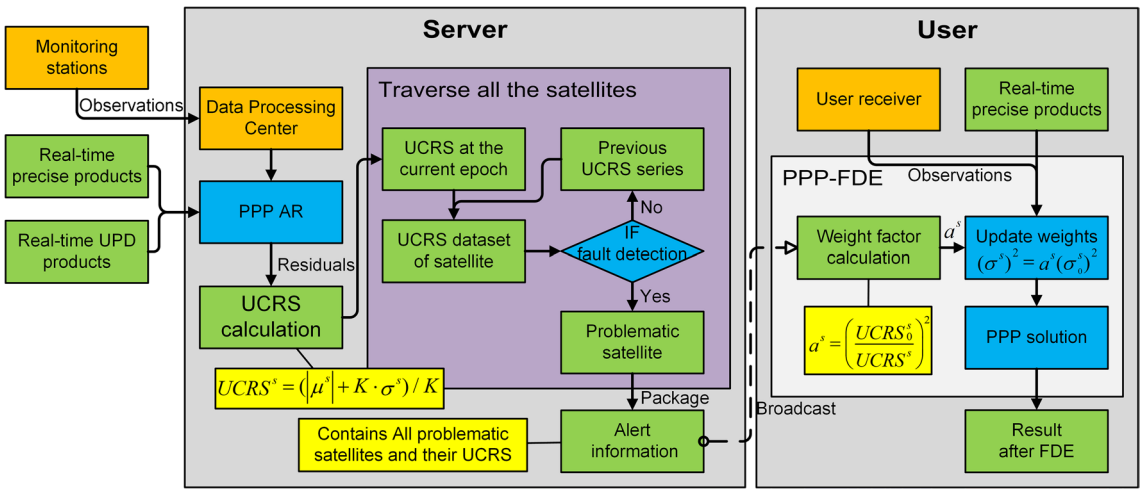

Fig. 3 Specific process design for quality monitoring system

problematic satellites and their UCRS are packaged together to form the alert information and broadcast.

Users can also perform PPP-FDE by receiving alert information broadcasted by the server. In PPP-FDE, the weight factor calculation module uses the alert information to calculate the weight factor of the problematic satellite through (9). By receiving the observations from the receiver and the real-time precise products, the weights of the observations are updated using the weight factor. Finally, after PPP with the updated weight information, users can get the positioning results after trouble removal.

Experimental data and processing strategies

According to the framework of the quality monitoring system proposed, we conducted two sets of experiments: the fault simulation experiment and the real-time precise product quality monitoring experiment to verify the feasibility and effectiveness of the proposed method. The data used in the experiment were obtained from the observation data of a large-scale station network in China. Figure 4 shows the distribution of the monitoring stations and experimental stations used, where the green markers represent monitoring stations and the red markers indicate experimental stations.

The data used in the experiment are shown in Table 1. The observations used are from base stations, including

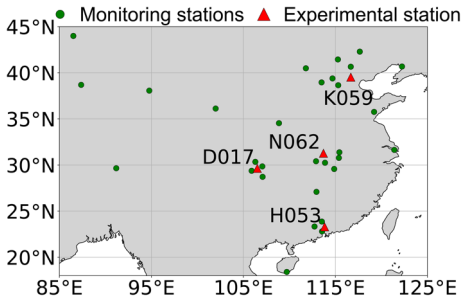

Fig. 4 Distribution of monitoring stations and experimental stations

January to July 2022 data. The broadcast ephemeris is derived from MGEX. In the fault simulation experiment, the precise product utilizes the final orbit and clock products from CODE. In the real-time precise product quality monitoring experiment, CNES's real-time clock products and ultra-rapid orbit products (www.ppp-wizard.net/products/REAL_TIME) are used. The satellite code biases are corrected by the DCB products from CAS, and the phase biases are corrected by the UPD products estimated by an open-source software called GREAT-UPD (https://geodesy.noaa.gov/gpstoolbox/) using hundreds of IGS stations around the world (Li et al. 2021).

Table 2 details the specific processing strategies used in the server PPP and the user PPP. At the server, in order to ensure data quality, it is necessary to adjust the satellite elevation angle limit to 15°, whereas the elevation cutoff angle is set as 7° at the users. The station coordinates are fixed to their a priori values with ambiguity fixed to integers at the server, while the coordinates are estimated in the epoch-wise kinematic mode at the user.

Fault simulation experiment

To validate the feasibility of this quality monitoring method, we conducted fault simulation experiments first. In the experiment, we utilized the observation data of 30 monitoring stations on January 5, 2022, along with the final precise products provided by CODE. The reason for selecting final precise products is their high accuracy and high reliability. This choice lets us avoid the impact of inherent potential faults in precise products during the experimental process. Experiments involve simulating various magnitudes of orbit and clock faults, and then detecting and identifying these faults using the proposed quality monitoring method.

This experiment simulates the step fault by adding a step error on the orbit and clock products at a certain epoch. Specifically, step error is introduced into the orbit or clock of certain satellites at epochs at every hour, as indicated in Table 3.

Table 1 Data used in the experiment

Data type	Data used	Data source	Sampling interval
Observation	Daily 5-s data	Base station	5 s
Navigation data	Broadcast ephemeris data	MGEX	–
Precise products	Final orbit	COD	5 min
	Final clock	COD	30 s
	Ultra-rapid orbit	CNES	5 min
	Real-time clock	CNES	30 s
Bias products	DCB	CAS	–
	UPD	Global IGS stations estimation	WL UPD, NL UPD 30 s

Table 2 Processing strategy of experiment

Items	Strategies	
GNSS system	GPS, Galileo and BDS	
Combination mode	Raw observations	
Data sampling interval	5s	
Elevation mask	Server	15°
	User	7°
Weight of observation	Weight of observation	
Phase ambiguities	Server	WL-L1 cascade partial fixing
	User	Float
Receiver coordinate	Server	Fixed
	User	Estimated in the epoch-wise kinematic mode
Ionospheric delays	Epoch-wise estimated for each satellite	
Tropospheric delays	Dry component	Modeled by Saastamoinen with Global Mapping function (GMF)
	Wet component	Random-walk estimated
Receiver clock	Epoch-wise estimated for each system and each frequency	

Table 3 Step errors involved to satellites

Time	prn	Time	prn	Time	prn
2:00	E24	9:00	C09	16:00	E01
3:00	E05	10:00	G09	17:00	G02
4:00	G10	11:00	C12	18:00	G05
5:00	C06	12:00	G30	19:00	E26
6:00	G32	13:00	E21	20:00	C13
7:00	E08	14:00	C11	21:00	G15
8:00	G27	15:00	C10	22:00	E12

The experiment involves introducing step errors to both orbit and clock measurements. For simulated orbit faults, it is necessary to add step errors in all three directions of the satellite orbit. The simulated orbit faults are divided into two groups, with errors of 10 cm and 5 cm, respectively. The simulated clock faults are divided into three groups, with errors of 0.3 ns, 0.2 ns, and 0.1 ns, respectively. In each group of experiments, using precise products contains step faults for server quality monitoring, detecting, and identifying fault sources.

Figure 5 presents the results of the experiment simulating a 10 cm orbit fault. The left panel displays the UCRS series of various satellites, indicating that the UCRS of a satellite unusually increases when it encounters a fault. By utilizing the Isolation Forest algorithm to detect outliers in UCRS, the fault time periods of each satellite can be obtained, as depicted in the right panel. In the figure, the gray-shaded periods indicate times when the satellite was not monitored, the green-shaded periods indicate times when the satellite was monitored and in a normal state, and the red-shaded periods indicate times when the satellite was identified as problematic. From the figure, it can be seen that the method can successfully identify all simulated step faults.

The same quality monitoring method was conducted for the other experimental groups to obtain alert information. The success rates of detecting artificially introduced step faults for each group were recorded and are shown in Table 4. It is observed that the method achieved a 100%

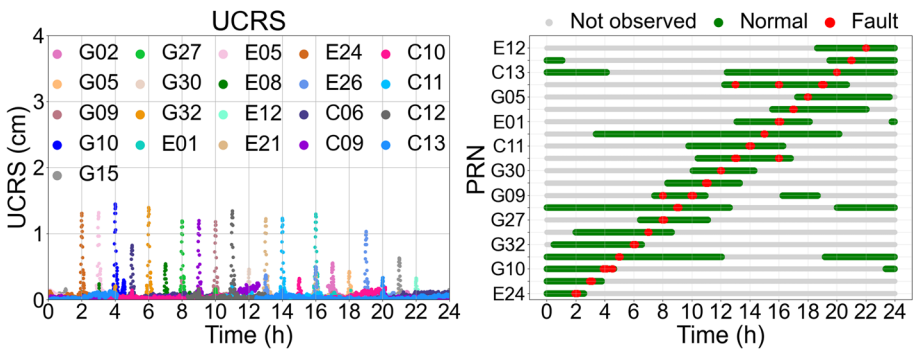

Fig. 5 Simulated step faults identification results. The left panel is the satellite UCRS series with 10 cm satellite orbit faults, and the right panel is the satellite fault period detected by the quality monitoring method

Table 4 Detection success rate of simulated orbit and clock faults of different magnitudes

Product	Group	Number of faults	Successful detection	Detection success rate (%)
Orbit	10 cm	21	21	100
	5 cm	21	20	95.24
Clock	0.3 ns	21	21	100
	0.2 ns	21	21	100
	0.1 ns	21	16	76.19

success rate in detecting 10 cm orbit faults and 0.3 ns and 0.2 ns clock faults. The success rate for detecting 5 cm orbit faults also exceeded 95%, while the success rate for detecting 0.1 ns clock faults reached only 76%. The experiments demonstrate that the method can successfully detect 5 cm orbit faults and 0.2 ns clock faults. However, its detection performance decreases for faults with even smaller magnitudes. Nevertheless, subsequent experiments revealed that faults of smaller magnitudes had little impact on the positioning results at the user.

The alert information generated by the server-side quality monitoring can be used for user-end positioning calculations. Simulations were conducted using experimental station data to represent user-end positioning. PPP and PPP-FDE positioning calculations were performed for each group of simulated faults. Figure 6 displays the results for station H053, where the left and right panels correspond to simulated 10 cm and 5 cm orbit faults, respectively. Due to satellite orbit error, the PPP positioning results were affected, resulting in divergence. In contrast, PPP-FDE effectively mitigated the positioning divergence caused by detected problematic satellites. Furthermore, the influence on positioning results was found to be smaller for 5 cm orbit faults compared to 10 cm orbit faults. The experiments demonstrate that, compared to PPP, PPP-FDE can mitigate the impact of faults on positioning results, leading to more stable and continuous positioning outcomes.

In conclusion, the simulation experiments have demonstrated the reliability of the quality monitoring method based on Isolation Forest for detecting and identifying faults in satellite. The method effectively detects orbit faults as small as 5 cm and clock faults of 0.2 ns. Furthermore, PPP-FDE was shown to mitigate the impact of faults on positioning, thereby enhancing the reliability of the positioning results.

Real-time precise product quality monitoring experiment

In this section, real-time clock and orbit products will be used for quality monitoring analysis. In this experiment, the server performs PPP AR positioning by receiving data from the monitoring station network and real-time precise products and bias products. This allows for the calculation of carrier phase residuals for each satellite, which are then used to generate the UCRS series. The Isolation Forest algorithm is subsequently employed to detect and identify problematic satellites, providing alert information.

The data from January to July 2022 have been processed, and six days (DOY 009, 011, 012, 014, 033, and 185), which exhibit obvious anomalies, is selected for detailed analysis. Figure 7 displays the detection results on DOY 009. The left panel showcases the UCRS series for some GPS satellites, while the right panel illustrates the identified time period during which these satellites had problems.

The users leverage the alert information disseminated by the server to perform PPP-FDE and enhance their own positioning quality. Consequently, experiments were conducted for data of DOY 009, 011, 012, 014, 033, and 185 using both PPP and PPP-FDE dynamic positioning. Comparative analysis was performed to evaluate the improvement brought about by PPP-FDE on the positioning results.

The results of the positioning comparison are illustrated in Fig. 8. The figure shows the series of positioning errors one hour before and after the abnormal positioning results on these days, which may be caused by faults in the precise

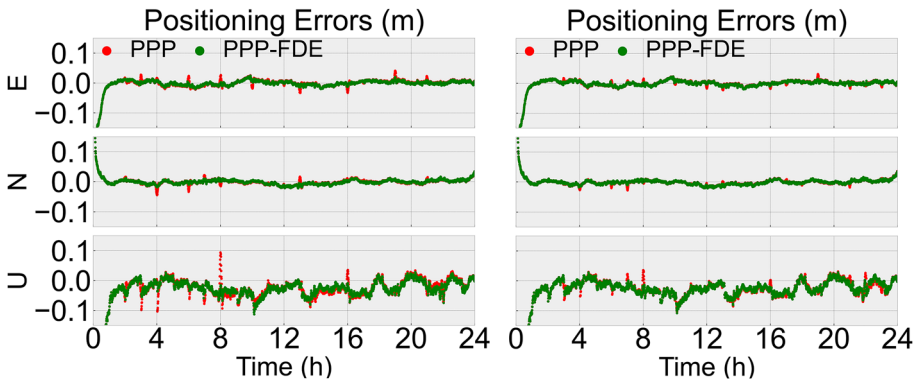

Fig. 6 Positioning error series of PPP and PPP-FDE. The left panel is the positioning error series of the H053 station of PPP and PPP-FDE when simulating a 10 cm satellite orbit fault, and the right panel is the results of simulating 5 cm satellite orbit fault

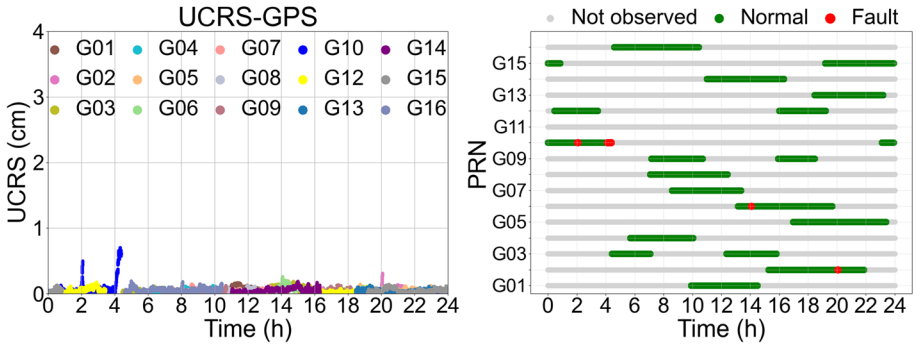

Fig. 7 Potential faults identification results. The left panel shows the UCRS series of the GPS part of the satellite on January 9, 2022, and the right panel shows the fault period detected and identified by the quality monitoring method

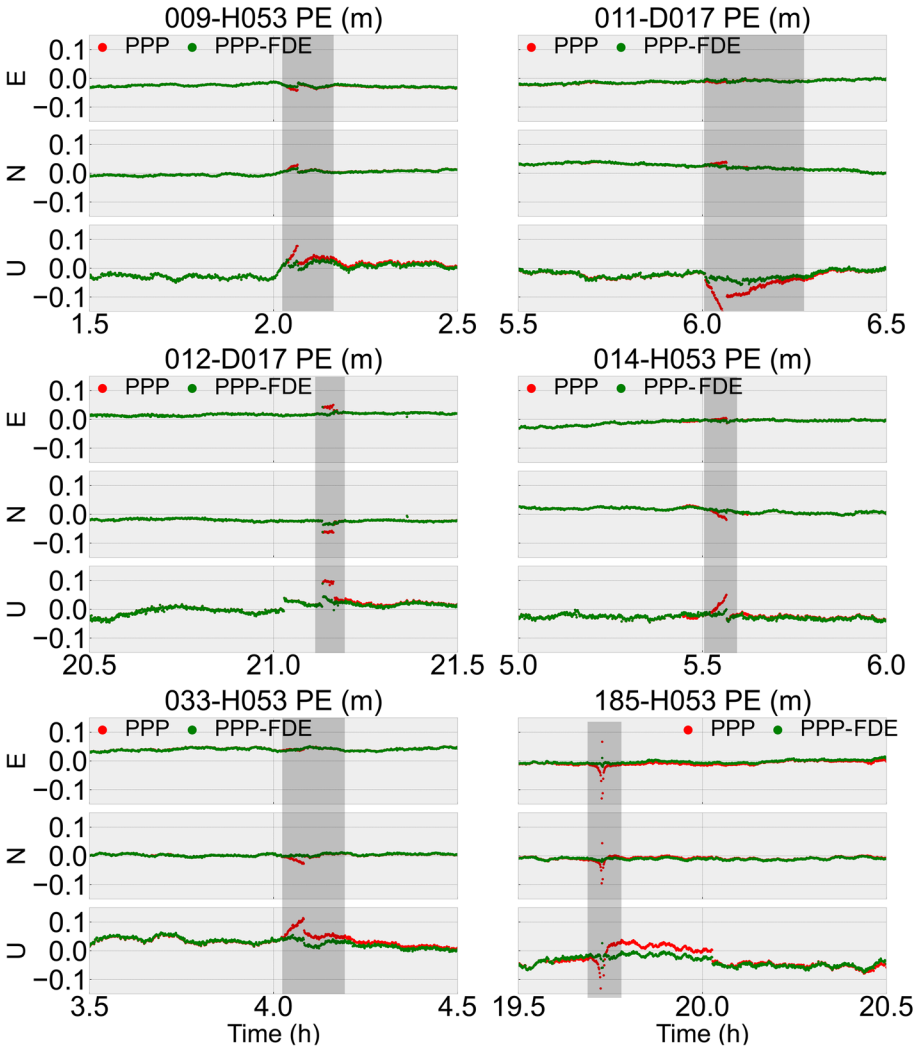

Fig. 8 Positioning error series of PPP and PPP-FDE one hour before and after the abnormal positioning results on DOY 009, 011, 012, 014, 033, and 185

product. After applying fault exclusion in PPP-FDE, there is a noticeable improvement in the stability of the positioning.

Table 5 lists the RMS of positioning errors for both PPP and PPP-FDE at the time of abnormal positioning results. The data indicate that compared to PPP, the positioning accuracy of PPP-FDE has been significantly improved in all three directions, particularly in the vertical direction, which is greatly affected by orbit and clock errors. In addition, Fig. 9 shows a 3D RMS comparison of PPP and PPP-FDE. It can be found that the 3D RMS of PPP-FDE has improved by 29%, 24%, 56%, 71%, 30%, and 60%, respectively.

To investigate the cause of discontinuities in PPP positioning results, this study provides an in-depth analysis of the precise clock and orbit products. The accuracy of real-time products can be assessed by differencing real-time clock and orbit products with final precise products.

Table 5 RMS statistics of the positioning error of PPP and PPP-FDE one hour before and after the abnormal positioning results on each day

DOY	PPP (cm)			PPP-FDE (cm)		
	E	N	U	E	N	U
009	2.91	1.12	3.36	2.62	0.80	1.79
011	6.46	1.13	15.2	6.50	1.21	10.64
012	4.15	5.91	9.03	1.77	3.33	3.43
014	0.60	1.63	3.76	0.26	0.28	1.15
033	4.15	0.98	6.34	4.14	0.46	3.37
185	1.95	1.38	5.32	0.63	1.11	1.95

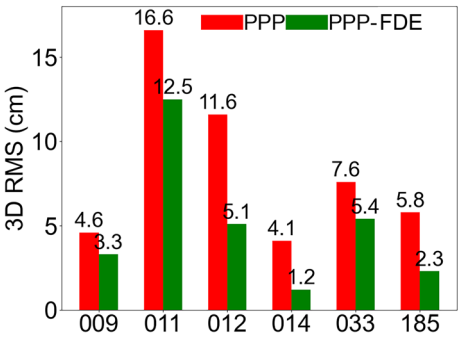

Fig. 9 3D RMS statistics of the positioning error of PPP and PPP-FDE one hour before and after the abnormal positioning results on each day

Figure 10 shows the anomaly analysis of the DOY 009 and 012 positioning results. In the figure, "CLK" represents the difference between CNES real-time clock products and COD final precise clock products, while "ORB_r" represents the difference in radial between CNES ultra-rapid orbit products and COD final precise orbit products. The plot only displays the satellites detected as problematic by the server. The left panel reveals that around 2:00 AM, the positioning error series exhibits an anomaly. During this period, two problematic satellites, G10 and G23, experienced a jump of about 6 cm in radial orbit difference values within 5 min after 2:00 AM, resulting in a slow drift in the positioning series. Simultaneously, the clock difference values of these two problematic satellites also experience a jump of about 8 cm, causing the positioning series to exhibit a discontinuity. In the right panel, at around 21:08 PM, there is also an anomaly in the positioning series. Among the three problematic satellites, their orbit products are all in a normal state. However, there has been a mutation of about 20 cm in the clock difference values of satellites E26 and E33, resulting in a jump in the positioning series. Large errors in real-time orbit and clock products may be caused by changes in the reference clock (Du et al. 2021). The analysis shows that the method successfully identifies potential faults in real-time precise products. Although there might be some false alarms, this hardly affects the improvement achieved by PPP-FDE on the positioning results.

Conclusions

We detail a server-side quality monitoring method aiming at detecting and excluding potential faults in satellite orbit and clock by leveraging the Isolation Forest algorithm to improve the performance of real-time PPP. The method involves meticulous statistical analysis of carrier phase residuals and the formulation of the UCRS parameter, facilitating anomaly detection using the Isolation Forest algorithm. Using the proposed method, the server can effectively detect and identify problematic satellites, generate alert information, and broadcast it in real time. In addition, a weighting scheme based on UCRS is proposed,

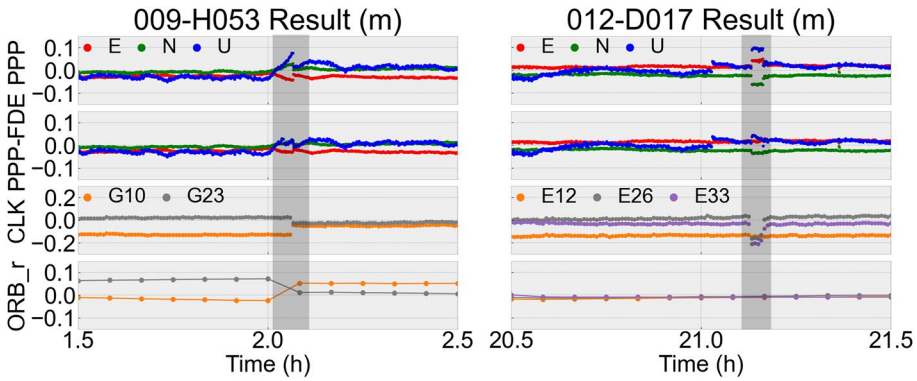

Fig. 10 PPP and PPP-FDE positioning series, the clock and orbit difference series of problematic satellites within one hour before and after the abnormal positioning results

which is beneficial to reduce the influence of problematic satellites on the positioning of the user.

The step faults of orbit and clock with different gradients are simulated in the experiments, and the quality monitoring method proposed is used to detect them. The results show that the detection success rate of the method is more than 95% for orbit faults larger than 5 cm and clock faults larger than 0.2 ns. The proposed method is also used to detect the potential faults of real-time precise products, and the analysis shows that it can effectively detect large errors in real-time orbit and clock. In addition, the UCRS-based weighting scheme is used to perform PPP-FDE on the data containing large errors. The statistical results show that the accuracy of PPP-FDE is significantly improved by 27–71% compared with the traditional PPP.

The method proposed, integrating the Isolation Forest algorithm for anomaly detection, offers distinct advantages over conventional server-side quality monitoring methods. Its capability is to effectively identify minor real-time precise product faults minimizing the impact of these faults on positioning outcomes, consequently enhancing the overall quality and stability of positioning results. While the monitoring stations were regionally confined to China in this study, future research endeavors could extend their coverage globally, enabling comprehensive and continuous monitoring of satellites across systems and benefiting users worldwide. At the same time, the method proposed can also be extended to real-time PPP-RTK to provide users with alert information.

Acknowledgements The algorithm implementation is based on the GNSS + REsearch, Application and Teaching (GREAT) software developed by the GREAT Group, School of Geodesy and Geomatics, Wuhan University. The numerical calculations in this paper have been done on the supercomputing system in the Supercomputing Center of Wuhan University.

Authors' contributions XXL, DL, and XL provided the initial idea and designed the experiments for this study; XXL, DL, and XL analyzed the data and wrote the manuscript; and JH, JW, and HG helped with the writing. All authors reviewed the manuscript.

Funding This work has been supported by the National Natural Science Foundation of China (No. 41974027, 42204017) and the special fund of Hubei Luojia Laboratory (220100006).

Data availability The datasets supporting this research are available from the corresponding author for academic purposes on reasonable request.

Declarations

Competing interests The authors declare no competing interests.

Ethical approval This manuscript does not report on or involve the use of any animal or human data or tissue.

Consent for publication All authors approved the final manuscript and the submission to this journal.

References

Dow JM, Neilan RE, Rizos C (2009) The international GNSS service in a changing landscape of global navigation satellite systems. J Geodesy 83:191–198. https://doi.org/10.1007/s00190-009-0315-4

Du Y, Wang J, Rizos C, El-Mowafy A (2021) Vulnerabilities and integrity of precise point positioning for intelligent transport systems: overview and analysis. Satell Navig 2(1):1–22. https://doi.org/10.1186/s43020-020-00034-8

El-Mowafy A (2018) Real-time precise point positioning using orbit and clock corrections as quasi-observations for improved detection of faults. J Navig 71(4):769–787. https://doi.org/10.1017/S0373463317001023

European GNSS Agency (2019) PPP-RTK market and technology report

Geng J, Bock Y (2013) Triple-frequency GPS precise point positioning with rapid ambiguity resolution. J Geodesy 87(5):449–460. https://doi.org/10.1007/s00190-013-0619-2

Geng J, Guo J, Meng X, Gao K (2020) Speeding up PPP ambiguity resolution using triple-frequency GPS/BeiDou/Galileo/QZSS data. J Geod 94(1):6. https://doi.org/10.1007/s00190-019-01330-1

İlçi V, Peker AU (2022) The kinematic performance of real-time PPP services in challenging environment. Measurement 189:110434. https://doi.org/10.1016/j.measurement.2021.110434

Ji R, Jiang X, Chen X, Zhu H, Ge M, Frank N (2022) Quality monitoring of real-time GNSS precise positioning service system. Geo-Spatial Inf Sci 26(1):1–15. https://doi.org/10.1080/10095020.2022.2070554

Kouba J, Héroux P (2001) Precise point positioning using IGS orbit and clock products. GPS Solutions 5:12–28. https://doi.org/10.1007/PL00012883

Li X, Ge M, Douša J, Wickert J (2014) Real-time precise point positioning regional augmentation for large GPS reference networks. GPS Solutions 18:61–71. https://doi.org/10.1007/s10291-013-0310-3

Li X, Li X, Yuan Y, Zhang K, Zhang X, Wickert J (2018) Multi-GNSS phase delay estimation and PPP ambiguity resolution: GPS, BDS, GLONASS, Galileo. J Geod 92:579–608. https://doi.org/10.1007/s00190-017-1081-3

Li X, Li X, Liu G, Feng G, Yuan Y, Zhang K, Ren X (2019) Triple-frequency PPP ambiguity resolution with multi-constellation GNSS: BDS and Galileo. J Geod 93:1105–1122. https://doi.org/10.1007/s00190-019-01229-x

Li X, Han X, Li X, Liu G, Feng G, Wang B, Zheng H (2021) GREAT-UPD: an open-source software for uncalibrated phase delay estimation based on multi-GNSS and multi-frequency observations. GPS Solutions 25:1–9. https://doi.org/10.1007/s10291-020-01070-2

Li X, Gou H, Li X, Shen Z, Lyu H, Zhou Y, Wang H, Zhang Q (2023) Performance analysis of frequency-mixed PPP-RTK using low-cost GNSS chipset with different antenna configurations. Satellite Navig 4(1):26. https://doi.org/10.1186/s43020-023-00116-3

Liu FT, Ting KM, Zhou Z (2008) Isolation forest. In: 2008 Eighth IEEE International Conference on Data Mining, Pisa, Italy, 15–19 December 2008, pp 413–422. https://doi.org/10.1109/ICDM.2008.17

Malys S, Jensen PA (1990) Geodetic point positioning with GPS carrier beat phase data from the CASA UNO experiment. Geophys Res Lett 17(5):651–654

Wang Y, Li R (2013) The analysis of character of user range accuracy. In: Proceedings CSNC 2013, Lecture Notes in Electrical Engineering, Berlin, Heidelberg, p 244. https://doi.org/10.1007/978-3-642-37404-3_24

Wang Y, Shen J (2020) Real-time integrity monitoring for a wide area precise positioning system. Satell Navig 1(1):1–10. https://doi.org/10.1186/s43020-020-00018-8

Wang Y, Li R, Zhao R (2015) Research of signal-in-space integrity monitoring based on inter-satellite links. Chin J Electron 24(2):439–444. https://doi.org/10.1049/cje.2015.04.036

Weinbach U, Brandl M, Chen X, Landau H, Pastor F, Reussner N, Rodriguez-Solano C (2018) Integrity of the Trimble® CenterPoint RTX Correction Service. In: Proceedings ION GNSS+ 2018, Institute of Navigation, Miami, Florida, USA, September 24–28, 1902–1909. https://doi.org/10.33012/2018.15971

Zhang W, Wang J, El-Mowafy A, Rizos C (2023) Integrity monitoring scheme for undifferenced and uncombined multi-frequency multi-constellation PPP-RTK. GPS Solutions 27(2):68. https://doi.org/10.1007/s10291-022-01391-4

Zumberge J, Heflin M, Jefferson D, Watkins M, Webb F (1997) Precise point positioning for the efficient and robust analysis of GPS data from large networks. J Geophys Res: Solid Earth 102(B3):5005–5017. https://doi.org/10.1029/96JB03860

Xingxing Li is currently a professor at Wuhan University. He completed his B.Sc. degree at the School of Geodesy and Geomatics in Wuhan University and obtained his Ph.D. at the Department of Geodesy and Remote Sensing of the German Research Centre for Geosciences (GFZ). His current research mainly involves GNSS precise data processing and its application for geosciences.

Da Liang is currently a master's candidate at Wuhan University. He received his B.S. degree from the School of Geodesy and Geomatics, Wuhan University, Wuhan, China, in 2022. His area of research currently focuses on GNSS precise positioning.

Xin Li is currently a postdoctoral at Wuhan University. She received a master's and Ph.D. degree from the School of Geodesy and Geomatics, Wuhan University, Wuhan, China, in 2018 and 2021, respectively. Her area of research currently focuses on GNSS precise positioning and multi-sensor navigation.

Jiande Huang is currently a Ph.D. candidate at Wuhan University. He has completed his B.S. and master' degree from the School of Geodesy and Geomatics, Wuhan University, Wuhan, China, in 2018 and 2021. His area of research currently focuses on GNSS precise positioning.

Jiaqi Wu is currently a Ph.D. candidate at Wuhan University. He has completed his B.S. and master' degree from the School of Geodesy and Geomatics, Wuhan University, Wuhan, China, in 2017 and 2020. His area of research currently focuses on GNSS precise orbit determination.

Hailong Gou is currently a master's candidate at Wuhan University. He received his B.S. degree from the School of Geodesy and Geomatics, Wuhan University, Wuhan, China, in 2021. His area of research currently focuses on GNSS precise positioning.